Xylella fastidiosa Infection and Ethylene Exposure Result in Xylem and Water Movement Disruption in Grapevine Shoots[1][OA]

Alonso G. Pérez-Donoso[2], L. Carl Greve, Jeffrey H. Walton, Ken A. Shackel, and John M. Labavitch*

Department of Plant Sciences (A.G.P.-D., L.C.G., K.A.S., J.M.L.) and Nuclear Magnetic Resonance Facility (J.H.W.), University of California, Davis, California 95616

It is conventionally thought that multiplication of the xylem-limited bacterium *Xylella fastidiosa* (*Xf*) within xylem vessels is the sole factor responsible for the blockage of water movement in grapevines (*Vitis vinifera*) affected by Pierce's disease. However, results from our studies have provided substantial support for the idea that vessel obstructions, and likely other aspects of the Pierce's disease syndrome, result from the grapevine's active responses to the presence of *Xf*, rather than to the direct action of the bacterium. The use of magnetic resonance imaging (MRI) to observe the distribution of water within the xylem has allowed us to follow nondestructively the development of vascular system obstructions subsequent to inoculation of grapevines with *Xf*. Because we have hypothesized a role for ethylene produced in vines following infection, the impact of vine ethylene exposure on obstruction development was also followed using MRI. In both infected and ethylene-exposed plants, MRI shows that an important proportion of the xylem vessels become progressively air embolized after the treatments. The loss of xylem water-transporting function, assessed by MRI, has been also correlated with a decrease in stem-specific hydraulic conductivity (K_S) and the presence of tyloses in the lumens of obstructed water conduits. We have observed that the ethylene production of leaves from infected grapevines is greater than that from healthy vines and, therefore, propose that ethylene may be involved in a series of cellular events that coordinates the vine's response to the pathogen.

Pierce's disease (PD) is a disease of grapevines (*Vitis vinifera*) caused by the xylem-limited bacterium *Xylella fastidiosa* (*Xf*). Vines affected by PD become nonproductive, declining in vigor and ultimately dying from the disease, generally within 2 years (Varela et al., 2001). PD emerged as a serious problem in California in the early 1990s when the glassy-winged sharpshooter (*Homalodisca coagulata* Say), a highly efficient vector native to the east coast, reached the southern part of the state. It became clear when several vineyards were lost to the disease, that PD posed a major statewide threat to the valuable grape and wine industries.

Hopkins (1989) suggested that a dysfunction of the water-conducting system due to vascular occlusion by increasing *Xf* populations is the main mechanism for pathogenesis in PD; although, the involvement of phytotoxins and plant growth regulators has been reassessed periodically. Tyloses, pectin gels (Fry and Milholland, 1990; Stevenson et al., 2004), and bacterial aggregates (Newman et al., 2003; Stevenson et al., 2004) have been observed plugging the xylem vessels of *Xf*-infected vines. Also, bacterial exopolysaccharide (EPS), sometimes called fastidian gum, has been mentioned as a cause of vessel occlusions (da Silva et al., 2001; Osiro et al., 2004; Stevenson et al., 2004). However, clear evidence of EPS plugging xylem vessels has not been provided and, currently, the idea is based largely on the presence in the *Xf* genome of a gene cluster, putatively encoding EPS synthesis (Simpson et al., 2000; da Silva et al., 2001; Scarpari et al., 2003) and microscopy observations showing obstructions, but providing no clear evidence that they were of *Xf* origin. The presence of bacterial aggregates has been reported in stems and specifically in leaf petioles but a recent work quantifying the size and distribution of bacterial colonies found that the majority of the colonized vessels contained few bacterial cells, and that vessel occlusion caused by *Xf* colonies was relatively uncommon (Newman et al., 2003). The occlusions found in leaf vessels are predominantly caused by pectin gels (Fry and Milholland, 1990), whereas in the stem, the plugging is due mainly to tyloses (Stevenson et al., 2004). Thus, it seems that pectin gels and tyloses, both of plant origin, are the main kinds of occlusions that plug xylem vessels and cause reduced water transport in *Xf*-infected vines.

The occurrence of vessel cavitations during the progression of PD could also partially explain the loss of water-conducting capacity in *Xf*-infected vines.

[1] This work was supported by the Pierce's Disease Control Program and the Glassy-Winged Sharpshooter Board (California Department of Food and Agriculture grant no. 03–0283 to K.A.S. and J.M.L.).

[2] Present address: Departamento de Fruticultura y Enología, Facultad de Agronomía e Ingeniería Forestal, Pontificia Universidad Católica de Chile, Vicuña Mackenna 4860, Santiago, Chile.

* Corresponding author; e-mail jmlabavitch@ucdavis.edu; fax 530–752–2278.

The author responsible for distribution of materials integral to the findings presented in this article in accordance with the policy described in the Instructions for Authors (www.plantphysiol.org) is: John M. Labavitch (jmlabavitch@ucdavis.edu).

[OA] Open Access articles can be viewed online without a subscription.

www.plantphysiol.org/cgi/doi/10.1104/pp.106.087023

Classical anatomical methods are not useful to reveal the presence of cavitations because they are destructive. Usually, two consecutive hydraulic conductivity (K_S) measurements, the first made at a low and the second at high pressure are used to estimate the percentage of embolized vessels in a stem or petiole segment. This technique was used in a study that did not find evidence of cavitations contributing to the loss of water conduction described in PD (McElrone et al., 2003). However, this method is indirect and is destructive, requiring shoot excision. In contrast, the utility of magnetic resonance imaging (MRI) to visualize cavitations has been demonstrated in recent work (Holbrook et al., 2001; Clearwater and Clark, 2003). Ethylene has been reported to mediate the formation of vascular occlusions in fungal vascular diseases (VanderMolen et al., 1983). Vines were exposed to ethylene to determine if this exposure, in the absence of *Xf*, was sufficient to trigger the development of vascular occlusions similar to the ones observed in *Xf*-infected vines. Evidence that ethylene alone can elicit the formation of vascular occlusions would suggest a role for ethylene mediating this process during PD development. Preliminary observations suggesting that ethylene production is elevated in infected vines support the idea that vessel obstructions, and probably other aspects of the PD syndrome, are the consequence of an active plant response to the presence of *Xf*, rather than to a direct action of the bacterium.

This study was performed as part of an effort to describe events in the development of PD. The specific objective was to use MRI to assess visually and nondestructively the occurrence of nonfunctional vessels as disease development progressed. There is a relatively long and somewhat variable time delay between *Xf* introduction and the appearance of visible vine symptoms (Varela et al., 2001). Thus, MRI was tested as a means to follow, over time, xylem-level consequences of infection in individual, asymptomatic vines and demonstrated the progressive occurrence of cavitated vessels in parallel with decreased water conductivity, measured destructively.

RESULTS

Stem Morphology

The vines used in the *Xf*-inoculation and ethylene-exposure experiments developed between fall and spring time and, as a consequence, grew continuously but slowly. Only one inoculated vine, analyzed at the end of the evaluation period (spring, 2004), presented external leaf PD symptoms at the base of the shoot. All the other vines did not show external symptoms or signs in shoot apices, leaves, or stems that could be attributed to the *Xf* population or response to ethylene. However, after the experiments were concluded, all the new shoots that grew after pruning the *Xf*-inoculated plants (shoots that had not been directly inoculated) exhibited typical PD symptoms. The lack of external symptoms in *Xf*-inoculated vines, even 7 months after inoculation, indicates also a slow infective colonization process by the bacteria. Therefore the images, hydraulic measurements, and other results from the inoculation experiment most likely describe the development of early PD symptoms in grapevine stems.

The total stem lengths of the shoots used in these experiments can be seen in Table I. Only the mean number of internodes for the *Xf*-inoculated vines (designated I) was statistically different from the means of the mock-inoculated controls (designated IC). There were no significant differences between infected vines and ethylene-treated vines (designated E) and their controls (IC and EC, respectively) with respect to the average lengths and diameters of the internode segments used for K_S measurements (Table I). In general, the vines used in the ethylene experiment were evaluated later in the growth season and they tended to exhibit larger internode diameters ($P = 0.0731$) and xylem cross-sectional areas ($P = 0.0205$) than the vines from the inoculation experiment. We found a linear relationship between the cross-sectional area of the stem (A_S) and the xylem cross-sectional area (A_X) measured in the same internodes. The cross-section area of the xylem is about half of that of the stem (Fig. 1). There were no statistical differences in A_S and A_X between the treated and control vines ($P > 0.05$). A_X was also analyzed as a function of the relative position at which it was measured along the stem; i.e. the number of internodes away from the tip (of the total length of the shoot). In all treatments A_X increased linearly away from the tip ($P < 0.001$ for all the treatments).

Use of MRI to Visualize Xylem Vessel Content

Previous studies have described the ability of MRI to visualize in vivo the occurrence of individual vessel

Table I. *Total lengths of the shoots, average internode lengths (per shoot), and average diameters of the stem segments used for K_S computations*

Means, standard errors (SES), and P values from a one-way ANOVA are shown. I, *Xf* inoculation; IC, mock-inoculated stems; E, ethylene exposure; EC, control for ethylene.

Measured Plant Parameters	*Xf* Inoculation				C_2H_4 Treatment			
	I	IC	SE	*P* Value	E	EC	SE	*P* Value
Total stem length (m)	0.774	1.131	0.139	0.095	0.849	0.982	0.063	0.176
Total stem length (N° internodes)	25.57	36.57	3.46	0.044	32.40	32.80	2.65	0.918
Average internode length (mm)	23.50	22.54	1.38	0.631	22.12	26.22	2.35	0.251
Average internode diameter (mm)	3.02	3.05	0.16	0.893	3.17	3.49	0.14	0.137

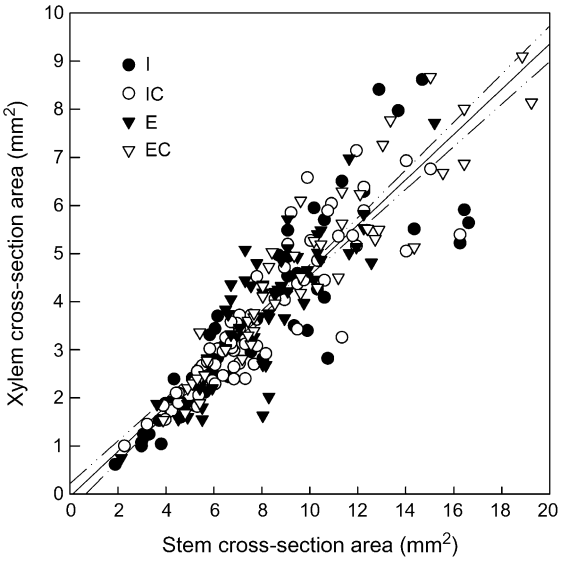

Figure 1. Linear regression between the cross-section areas of the stem (A_S) and the xylem tissue (A_X), the confidence interval ($\alpha = 0.05$) is also shown. $A_X = -0.058114 + 0.4708913\ A_S$ ($P < 0.0001$; $r^2 = 0.8038$); the slope is not significantly different from 0.5.

cavitations caused by large pressure gradients in the xylem during water deficit (Holbrook et al., 2001; Clearwater and Clark, 2003). The sequence of images in Figure 2 demonstrates that the MRI protocol used herein can reveal the presence of cavitations in large zones of the xylem. The cross section of a healthy, intact stem is depicted in Figure 2A; the radially oriented arrays of bright circles between the central pith (dark) and the ring of vascular cambium represent groups of functional vessels. The same stem section shows the development of dark zones after a transverse cut was made through approximately 70% of the stem cross-sectional area to cause most of the vessels to embolize (Fig. 2B). Dark zones appear where cavitated vessels are located because the magnetic signal from water is lost in these vessels. After the stem segment was examined by MRI, it was completely excised from the vine and flushed with pressurized water to refill cavitated vessels. MRI showed that the dark zones had been replaced by the bright signal of water-filled vessels (Fig. 2C). Finally, after the same segment had been flushed with air to empty the vessels of water, most of the xylem disc appeared dark (Fig. 2D).

To understand the limits of the interpretations of changes in vessel functionality that could be made from examination of the MRIs, the signal intensities were compared for glass tubes filled with pure water, a saline solution (KCl), and a pectin gel. The signal intensities of glass tubes filled with these three materials were quite similar (Fig. 3). This suggests that MRI cannot differentiate between vessels filled with regular xylem sap and vessels filled with pectic materials from plant gels. It also indicates that the occurrence of dark zones where water-filled vessels are expected should be interpreted as regions where vessels are air filled, not gel filled.

MRI Reveals Vessel Cavitation in Externally Asymptomatic *Xf*-Infected and Ethylene-Gassed Vines

MRI is capable of showing xylem disruption and nonfunctional vessels well before external symptoms appear in *Xf*-infected plants. Dark zones, indicative of vessel embolisms, are typically observed in images of infected vines. The image in Figure 4A shows an infected plant at a basal internode where leaf symptoms of PD were apparent. Closer to the stem apex, at a point where the leaves showed no PD symptoms, MRI also reveals the presence of several empty vessels (Fig. 4B). The contrast of these images with those for a healthy stem is evident; in healthy stems the xylem appears as a hollow disc full of bright images indicating water-filled vessels (Fig. 2A).

A time course series of images taken after imposing the treatments revealed the progressive development of dark zones in both *Xf*-inoculated and ethylene-treated vines. Initial signs of embolisms in the xylem can be seen 18 to 54 d after inoculating the vines with *Xf* (Fig. 5). The dark, cavitated zones increase in size over time until they become an important proportion of the total area of the xylem. A similar progression was observed in ethylene-gassed vines from two independent experiments (Fig. 6). MRI showed the presence of cavitations between 19 to 47 d in young vines (Fig. 6, A–C) and between 10 to 19 d in mature vines gassed with ethylene (Fig. 6, D–F).

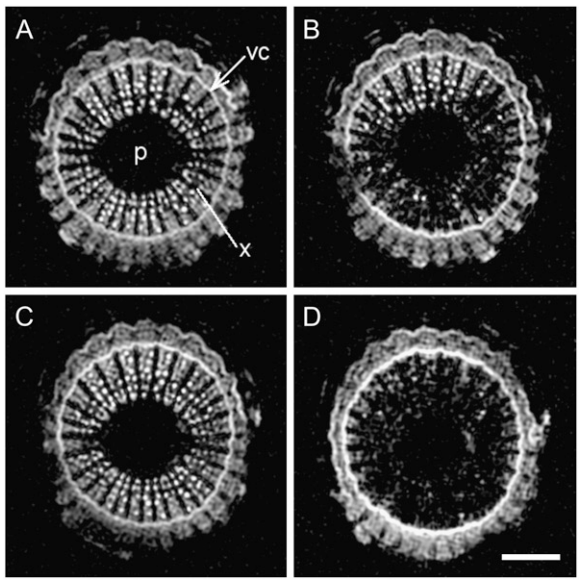

Figure 2. A, Image of an intact stem segment in a healthy shoot. B, Image of the same stem portion after 70% of the cross section has been removed below it. C, The same stem segment after pressurized water was introduced. D, Stem segment after flushing with air to completely empty the xylem vessels. vc, Vascular cambium; x, xylem tissue; p, pith. Scale bar = 1 mm.

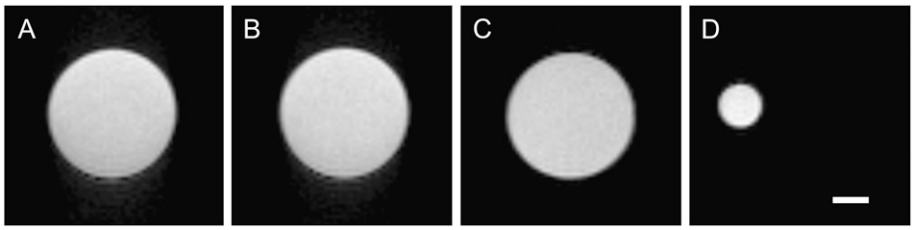

Figure 3. Glass tubes containing either distilled water (A), 10 mM KCl solution (B), or a pectin gel (C) were put in the magnet at the same time and imaged. D, Small glass capillary filled with a pectin gel next to an empty glass tube that does not appear in the image. The signal intensities ±1 SD were 195.4 ± 15.2, 202.8 ± 12.2, and 196.1 ± 4.4 for A, B, and C, respectively. Scale bar = 1 mm.

A higher proportion of the images taken along the stems of *Xf*-inoculated (I) and ethylene-treated vines (E) was categorized as exhibiting large cavitations (L) in comparison with the images of the controls (IC and EC; Fig. 7). This increase in the proportion of images depicting large, dark zones implied a reduction in the proportion of images classified as presenting normal, water-filled, and presumably functional xylem (N). The χ^2 likelihood-ratio test indicated that the distributions of the proportions of images exhibiting large, dark zones or normal-looking xylem were significantly different among the group treatments (Fig. 7). A correspondence analysis confirmed that *Xf*-inoculated and ethylene-treated vines were more closely associated with accumulations of empty (dark) vessels in the xylem, whereas the control groups were clearly associated with images of normal, water-filled xylem conduits (Fig. 8). A comparison by internodes shows that both *Xf*- and mock-inoculated plants presented a high proportion of images exhibiting large, dark zones near to the base of the stem where inoculation or needle penetration during mock inoculation had occurred (internode zero in Fig. 9). Even 7 months after treatment, MRI showed inoculation-related cavitations extending frequently up to two internodes above the inoculation site (Figs. 9 and 10). If an internode was present below the inoculation point, generally, it also exhibited cavitated vessels (Fig. 9). In most of the other internodes, *Xf*-infected vines presented a higher proportion of large, dark zones and a lower proportion of normal-looking xylem than did the controls (IC). These differences were significant at internodes 10 and 12 (Fig. 9). A similar trend was observed for ethylene-gassed plants and their controls (EC) in which the biggest differences were also found in the distal halves of the stems, at internodes 14, 18, and 20 (Fig. 11).

Two of the vines that had been inoculated with *Xf*, and then were examined using MRI prior to the appearance of external PD symptoms and subsequent dissection for K_S assessments, exhibited only minor, internal xylem disruptions. The stems of these vines (designated I-N in the result description for K_S measurements) presented a distribution of the category proportions intermediate between *Xf*- and mock-inoculated plants (N = 35.29%, S = 47.06%, and L = 17.65%). This proportion was not significantly different from that of mock-inoculated vines ($P = 0.0682$, χ^2 likelihood ratio).

Xf Infection and Ethylene Exposure Reduce Water-Transporting Capacity of Stems

The impression of a loss in xylem water-transporting function that is given by the MRIs of *Xf*-inoculated and ethylene-gassed vines was confirmed by subsequent destructive measurements of water flow rates and the calculations for the specific hydraulic resistivity (ρ_S) of whole stems (ρ_{STEM}), and for the components of ρ_{STEM}, ρ_{NODE}, and ρ_{INT} (Fig. 12). This difference was not as clear in the inoculation experiment as it was in the ethylene experiment. The difference between the means for ρ_{STEM} of *Xf*-inoculated and control vines was not statistically significant, even when the mean ρ_{STEM} for *Xf*-inoculated plants was more than 3-fold higher than that for the control vines (IC). This was also true for the mean differences in ρ_{NODE} values for *Xf*- and mock-inoculated vines (Fig. 12). However, *Xf*-inoculated plants exhibited a ρ_{INT} that was significantly higher than that of the control vines. It was not possible to include one symptomatic vine in the calculations for ρ_S because it presented no flow ($K_S = 0$) and therefore its ρ_S was calculated to be infinitely large. In contrast, ethylene-gassed vines presented significantly higher means than the controls (EC) for ρ_{STEM}, ρ_{NODE}, and ρ_{INT}.

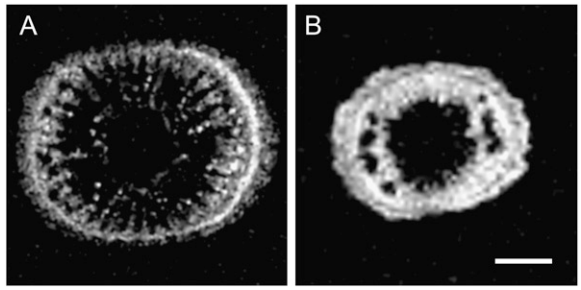

Figure 4. MRI of a *Xf*-infected stem in a basal internode (A) and closer to the apex (B). Bright spots between the central pith (dark) and the ring of vascular cambium show functional vessels. Dark zones within the vascular tissue indicate areas in which vessels are not water filled (compare the image to the healthy stem in Fig. 2A).

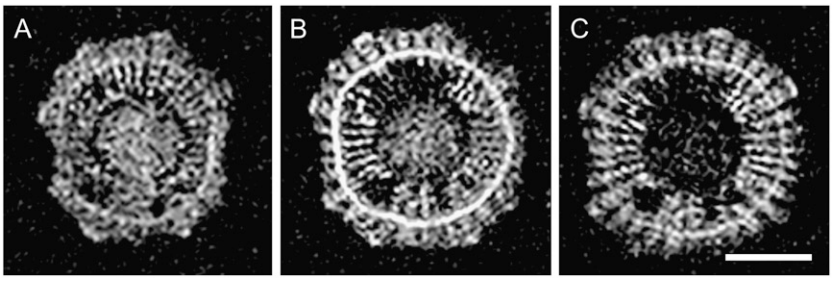

Figure 5. Temporal image sequence of an *Xf*-inoculated vine. Images were taken at the same internode 18 (A), 54 (B), and 97 d (C) after inoculation (September, 2003). The progressive development of dark zones due to the presence of embolized vessels is clear from A to C. Images are shown with approximately the same orientation with respect to each other. Scale bar = 1 mm.

Additionally, it was very clear that most of the resistivity to water movement in the stems (ρ_{STEM}) was due to the resistivity encountered at the nodes (ρ_{NODE}) and that for all treatments, ρ_{NODE} was much higher than ρ_{INT} (Fig. 12). The K_S measurements used to calculate ρ_S were collected over a period of 5 months, however no relationship was found between the evaluation dates and K_S or ρ_S values ($P > 0.05$). Since the majority of the stem hydraulic resistivity resided at the nodes, K_S values for whole stems were also expressed in terms of the number of nodes rather than stem lengths. The values calculated in this way correlated highly with the original K_S expressed per unit length of stem ($r^2 = 0.9123$) and gave the same experimental results.

In comparison with the controls (IC and EC), *Xf*-inoculated and ethylene-gassed vines (I and E) exhibited a reduction in K_S for individual internodes at specific internode positions along the stem (Fig. 13). *Xf*- and mock-inoculated vines presented a sharp drop in K_S at the inoculation point (internode 0) due to cavitations produced by the pin-prick inoculation technique (Figs. 9 and 10). I-N represents K_S for two vines that were inoculated with *Xf* but did not show external or internal (MRI) disease symptoms. The I-N vines had a higher mean K_S than the mock-inoculated control vines, presenting the highest K_S values for individual plants in the inoculation experiment (Fig. 13A). I-N vines were removed from the statistical analysis for K_S, and the comparison was done only using *Xf*-inoculated and control (mock-inoculated) vines. *Xf*-inoculated vines demonstrated a major reduction in K_S with respect to the controls from internodes 3 to 7, and at internode 16. Following treatment, ethylene-gassed vines presented significantly lower K_S

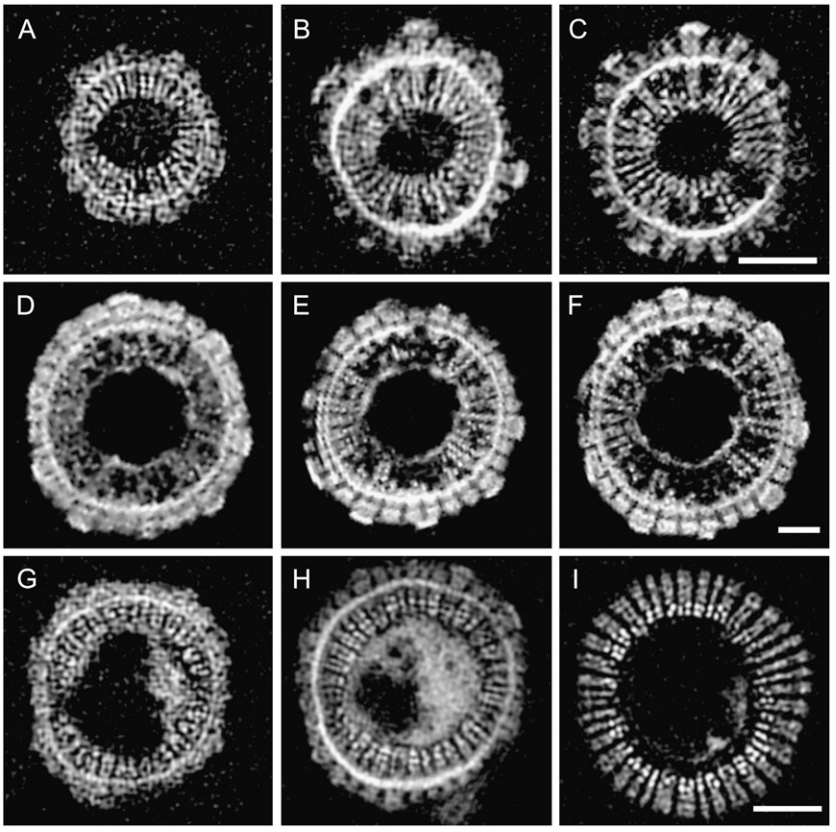

Figure 6. Temporal image sequences for two vines from two different ethylene-gassing experiments (A–C and D–F). Images were taken at the same internode 19 (A), 47 (B), and 61 d (C) after treatment (September, 2003); substantial growth occurred in this internode from A to B. Images from a previous experiment were taken 10 (D), 19 (E), and 39 d (F) after treatment (January, 2003). The progressive development of dark zones due to the presence of embolized vessels is clear from left to right in both image sequences. Temporal image sequence for a control (nongassed) vine 19 (G), 47 (H), and 136 d (I) after starting the experiment (September, 2003). Images for the same internodes are shown with approximately the same orientation with respect to each other. Scale bars = 1 mm.

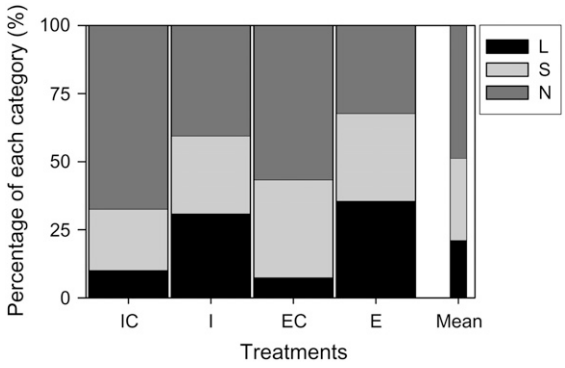

Figure 7. The mosaic plot depicts the percentages of the image categories N, S, and L for each treatment. The categories were defined in the "Material and Methods" section as normal-looking xylem (N), small cavitations (S), and large cavitations (L). The treatments were labeled IC (control for inoculation), I (*Xf* inoculated), EC (control for ethylene), and E (ethylene-gassed). Treatments E and I show a higher percentage of L and a lower percentage of N than the controls. The narrow bar to the right is the mean category percentage across all treatments. The distribution of the category proportions for all treatments was analyzed using the likelihood-ratio χ^2 test, which concluded that the treatments have different pattern distributions ($P = 0.0002$); n was 49, 42, 53, and 59 internode images for IC, I, EC, and E, respectively. Images depicting dark zones due to needle inoculation were not considered in the analysis of IC and I treatments.

than control plants (EC) from the base of the stem (internode 0) up to internode 5, and also at internode 15 (Fig. 13B).

Xf Infection and Ethylene Exposure Induce Vascular Occlusion Formation

Light microscopy observation of stem sections revealed that tyloses and pectin gels were more common in *Xf*-inoculated and ethylene-gassed vines than in the controls (data not shown). This is consistent with previous observations made on ethylene-gassed vines (S. Lurie, L.C. Greve, P. Bates, and J.M. Labavitch, unpublished data) and with reported data from *Xf* infection (Fry and Milholland, 1990; Stevenson et al., 2004). The internal anatomy of internodes from one of the asymptomatic I-N vines was examined under the microscope. This vine presented about 10 occluded vessels at the inoculation site, and very few occluded vessels (from 0–3) in other internodes. On the other hand, the comparable examination of a visually symptomatic vine that had been inoculated at the same time as the I-N vine examined, presented frequent occlusions in all its internodes. However, the proportion of occluded vessels in the symptomatic vine did not exceed 25% of vessels observed in any of the cross sections of internodes. As also reported by Mollenhauer and Hopkins (1976), amorphous materials that stained positive for pectins can be seen in *Xf*-infected vines either completely filling vessels, as free materials in vessel lumina, or lining the cell wall of vessels that are filled with tyloses.

Xf Infection Induces Ethylene Production in Leaves

Symptomatic and asymptomatic leaves taken from *Xf*-infected vines generated more ethylene than leaves taken from healthy vines (Fig. 14). Only the amount of ethylene produced by visually symptomatic leaves was statistically different from the amount produced by healthy leaves over a 24 h period.

DISCUSSION

MRI is very useful for visualizing the progression of changes in the internal vascular anatomy of grapevine stems because it is nondestructive. In MRI cross sections, the vascular cambium and water-filled xylem conduits located between the parenchyma rays appear bright and clearly distinguishable as individual conducting elements. The phloem tissue also appears bright and is readily discernible in young internodes prior to periderm differentiation. Once the periderm has formed, the vascular cambium and, especially, the phloem tissue are more difficult to distinguish. The parenchyma cells from the rays and pith are usually dark, but in the younger, more apical internodes both pith and xylem rays often appear bright, making it more difficult to distinguish individual xylem conduits (Figs. 5 and 6).

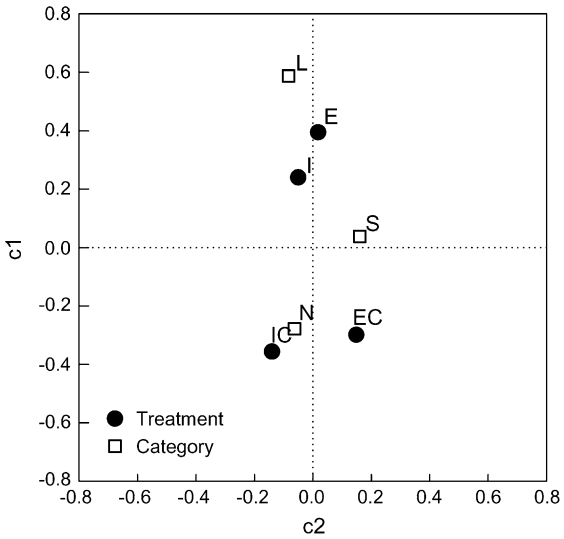

Figure 8. The correspondence analysis for the proportions of categories (N, S, and L) across treatments (IC, I, EC, and E) indicates that most of the variation (92%) of the response variable (category) happens in the c1-axis. L, S, and N categories align, respectively, from the positive (top) to the negative range of the c1-axis, establishing the directionality of the response. Thus the treatments located in the c1-axis positive range (I and E) are associated with the L category, and treatments in the negative range (IC and EC) are associated with the N category. The c2-axis explains only about 8% of the variability in the category variable. L and N are located fairly neutrally in the c2-axis whereas S locates in the positive range. Thus treatments in c2-axis positive range, like EC, are more associated to the S category. Images depicting dark zones due to needle inoculation were not considered in the analysis of IC and I treatments.

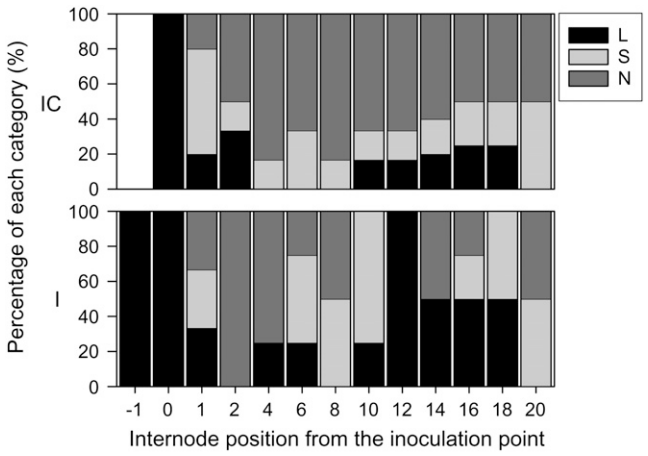

Figure 9. The mosaic plot depicts the percentages of the image categories normal (N), small (S), and large (L) for individual internodes along the stems. The treatments were labeled IC (control for inoculation) and I (*Xf* inoculation). I shows a higher percentage of L and a lower percentage of N than IC. The distribution of the category proportions was analyzed using the likelihood-ratio χ^2 test, which concluded that the treatments have different pattern distributions at internodes 10 and 12 ($P = 0.0453$ and 0.0146); n between 4 and 6 for IC, and between 3 and 4 for I.

Although the precise cause of the differences in brightness of stems imaged at different developmental stages is not known, it is likely that differences in tissue water content and water distribution might be related to the phenomenon. The epidermis appears very bright in young stems but as the more suberized and less hydrated periderm develops the brightness at the stem's periphery decreases (Fig. 6, I–H). Similarly, the brightness that can be observed in the pith and most of the xylem of younger, more apical internodes could be explained because young xylem conduits are mostly protoxylem, with walls composed mostly of primary cell wall. Thus, it is likely that these conduits are more permeable to radial water movement than older conduits; perhaps this allows the space between cells to become filled with water producing the brighter images observed with MRI.

The utility of MRI for visualizing cavitations in xylem conduits has been demonstrated in our experiments as well as in previous work (Holbrook et al., 2001; Clearwater and Clark, 2003). The MRI techniques used in the present study allowed the detection of conspicuous cavitations in the stems of *Xf*-infected and ethylene-gassed vines. This finding stands in contrast to previously published information (McElrone et al., 2003) indicating that cavitations do not play a role in reducing the water movement capacity of *Xf*-infected stems. This discrepancy could be explained because the period of the growing season in which the sampling was done might not have been adequate to detect cavitations, as suggested by McElrone et al. (2003). That work also used a rather high initial pressure of 80 kPa to measure the native hydraulic conductance as the percentage loss of conductance was estimated. This is in contrast to pressures of 7 to 10 kPa used in other studies (Hacke et al., 2000; Lo Gullo et al., 2000), and may have led to the refilling of embolized vessels, thus masking cavitations that were initially present. The results presented here are in agreement with evidence of embolisms preceding the formation of vessel occlusions in Dutch elm disease (Newbanks et al., 1983).

An observation that has not been described before is that when imaging artificially induced cavitations (Fig. 2) or cavitations in diseased stems (Fig. 4), we frequently found that the weaker signal from tissue that surrounded the vessels as well as the stronger, well-defined signals from individual vessels disappeared. This weaker signal may have originated from water stored in intercellular spaces and xylem fibers located between the water conduits (Tyree and Zimmermann, 2002); although the cause of its disappearance upon vessel cavitation is not clear from the studies thus far.

Despite the high variation in K_S and ρ_S among different plants, the error associated with the individual measurements on excised stem segments was negligible, thus the SEs appear to reflect true biological variability. Examinations of the *Xf*-inoculated vines revealed a gradation of the early stages of PD infection, but the vines were not displaying external disease symptoms when the destructive K_S tests were performed. This great disparity in symptom development along the stem, moving away from the point of inoculation that is revealed by the MRI analysis, helps to explain the large variability found in ρ_S measurements, and the fact that differences in the means for ρ_{STEM} and ρ_{NODE} between *Xf*- and mock-inoculated stems were not statistically significant. It is necessary to indicate that when K_S is measured in visually symptomatic shoots, the water flow through the whole stem is negligible and generally $K_S = 0$. This point is made clear in the measurements made on the only visually symptomatic shoot analyzed in this experiment. Even though ρ_{NODE} was much larger than ρ_{INT} in all the

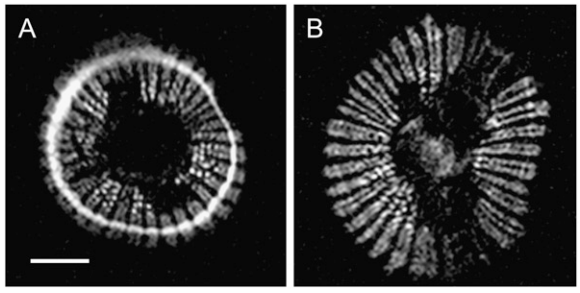

Figure 10. Images taken at the inoculation sites of a mock-inoculated (A) and a *Xf*-inoculated vine (B). Both vines were inoculated using a syringe needle to puncture the stem as far as the xylem, once through each of three droplets of inoculum that were placed in a shallow spiral around the stem circumference. Scale bar = 1 mm.

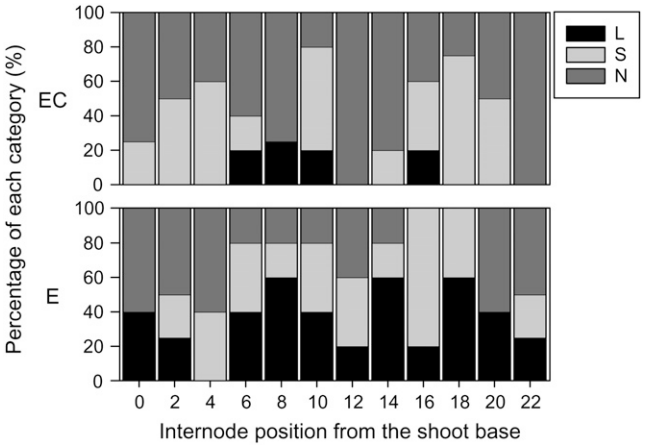

Figure 11. The mosaic plot depicts the percentages of the image categories normal (N), small (S), and large (L) for individual internodes along the stems. The treatments were labeled EC (control for ethylene) and E (ethylene exposure). E shows a higher percentage of L and a lower percentage of N than EC. The distribution of the category proportions was analyzed using the likelihood-ratio χ^2 test, which concluded that the treatments have different pattern distributions at internodes 14, 18, and 20 ($P = 0.0477$, 0.0597, and 0.0597); n between 2 and 5 for EC, and between 4 and 5 for E.

stems analyzed, at early stages of PD infection the only significant differences in resistivity between *Xf*-inoculated and control plants are found in the ρ_{INT} component. This suggests that tyloses and gels that plug the vessels, occlusions which would not have been removed during the K_S tests, are located preferentially at the internodes.

Mock-inoculated vines exhibited the development-related changes in K_S along the stem that have been described previously for grapevine internodes. K_S is usually higher in the middle portion of the stem and it decreases toward the base and tip of the shoot, being especially clear in the apical internodes (Schultz and Matthews, 1993). However, *Xf*-inoculated vines displayed an anomalous pattern for K_S along the stem, presenting minimum values in the middle and higher values toward the tip, where K_S values for *Xf*- and mock-inoculated stems were similar. Ethylene control stems presented higher K_S overall than did ethylene-treated stems but, as in the inoculation experiment, these differences were most significant at the internodes located closer to the base rather than toward the apex.

However, MRI revealed that in relationship to the controls (IC and EC), *Xf*-inoculated and ethylene-gassed vines (I and E) had a higher proportion of the dark zones associated with cavitations in the images taken at the apical portions of the stems. The discrepancy in the location of the xylem anomalies detected by MRI and K_S tests indicates that physical occlusions that obstruct the water flow throughout the vessels are more likely to be located in the internodes at the base of the stems, and that cavitations are predominantly located in the more apical internodes. In vines that have been needle inoculated at the stem base, PD symptoms develop sequentially from the inoculation point to the upper parts of the shoots, although traditional anatomical studies indicate that tyloses seem to develop in the stems only after bacteria, gum, and tyloses have been detected in leaves (Stevenson et al., 2004). This lagging in development of internal stem symptoms with respect to leaf symptoms could be explained because tyloses form in the stems only after the vessels become embolized and not functional. In our experiments, the presence of cavitations in the apical regions and tyloses in the basal regions may suggest that cavitations precede and, possibly, trigger the formation of tyloses in infected shoots. Thus, our data and the data from Stevenson et al. (2004) can be interpreted as consistent with the suggestion that tylose formation depends on prior vessel cavitation (Tyree and Zimmermann, 2002). This is a reasonable scenario, particularly if the cavitations were identified in the same vessels, information that MRI analysis alone does not provide. However, a recent study by Sun, Matthews, and Rost (personal communication) suggests that, in some cases, tyloses can form readily in grapevine vessels that are water filled. It seems reasonable to propose that if tyloses that completely close off vessels, as shown for PD-infected grapevines (Stevenson et al., 2004), developed in water-filled, functional vessels, their formation would quickly trigger cavitations in a position apical to the blockage. Our

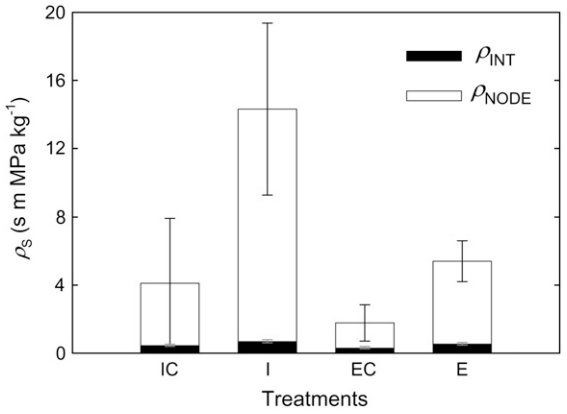

Figure 12. Specific hydraulic resistivities (ρ_S) for vines inoculated with *Xf* and exposed to ethylene. Total bar height represents ρ_S for whole stems (ρ_{STEM}). The resistivity components for nodes (ρ_{NODE}) and internodes (ρ_{INT}) are also shown. The error lines (ρ_{STEM} in black, ρ_{INT} and ρ_{NODE} in gray) correspond to ± 1 SE for the comparisons between the means of the treatments and their respective controls (one-sided ANOVA). I and IC did not show statistically significant differences for ρ_{STEM} and ρ_{NODE} ($P = 0.1351$ and 0.1630). However, I exhibited a significantly higher ρ_{INT} value than IC ($P = 0.0265$, $n = 4$ and 7 for I and IC, respectively). Ethylene-gassed vines (E) had significantly higher ρ_{STEM}, ρ_{NODE}, and ρ_{INT} values than the controls (EC; $P = 0.0302$, 0.0374, and 0.0397; $n = 4$ and 5 for E and EC, respectively). Regardless of the treatment, ρ_{NODE} is higher than ρ_{INT}, and it is the major component of ρ_{STEM} (two-sided ANOVA, $P < 0.0001$, $n = 20$).

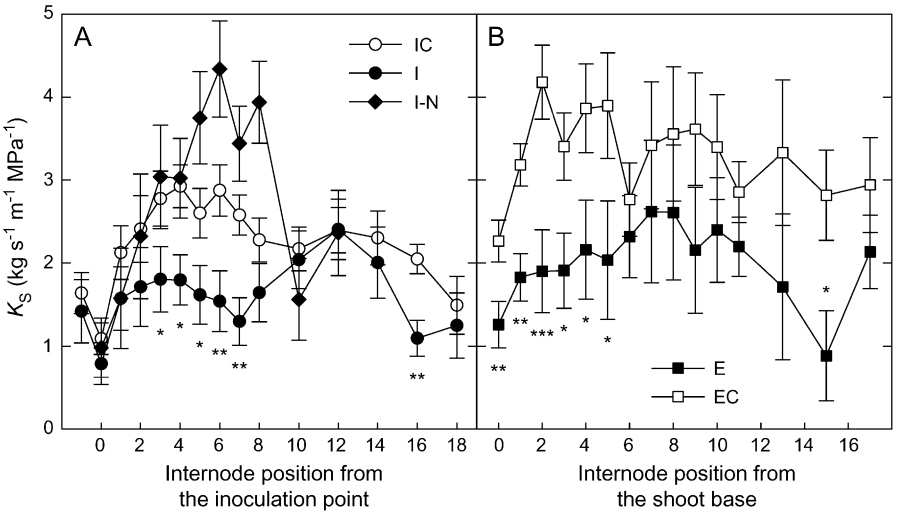

Figure 13. Specific hydraulic conductivities (K_S) for individual internodes (±1 SE) in grapevine stems. A, Vines inoculated with *Xf* (I) showing xylem disruptions detected by MRI, *Xf*-inoculated vines with normal xylem appearance (I-N), and controls (IC). The comparison was only made between I and IC. B, Vines exposed to ethylene (E) and controls (EC). A one-sided ANOVA test was used to determine whether the treatments I and E had significantly lower means than their respective controls IC and EC (n between 3 and 7 for I and IC, and between 3 and 5 for E and EC). The symbols *, **, and *** indicate statistical significance at a given internode position with probability inferior to 0.05, 0.01, or 0.001, respectively.

tests (Fig. 3) indicate that dark spots in MRIs represent cavitations rather than pectin gels. However, it is not clear whether a section through a tylose would be seen as a dark spot, similar to the dark parenchyma cells that border vessels, or as a bright spot. A more specific testing of the potential requirement of cavitation to permit tylose development would require use of parallel MRI and traditional histological studies and these are under way.

Xf has several genes whose sequences are similar to genes in other bacteria that encode cell wall-degrading polyglacturonase and β-1,4-glucanase (Wulff et al., 2003), but data for the presence of these enzymes in culture and in infected vines have been developed only recently (Agüero et al., 2005; M.C. Roper, L.C. Greve, A.G. Pérez-Donoso, and J.M. Labavitch, unpublished data). The dimensions of individual *Xf* cells vary from 250 to 500 by 1,000 to 4,000 nm (Mollenhauer and Hopkins, 1974); which make them much larger than the pores in the pit membranes that separate two neighboring vessels, measured to be 5 to <20 nm during spring and early summer (A.G. Pérez-Donoso, L.C. Greve, and J.M. Labavitch, unpublished data). Thus, it is possible that *Xf* uses plant cell wall-degrading enzymes to open up the pores and facilitate its movement from one vessel to the next (Fry and Milholland, 1990; Newman et al., 2003, 2004; Osiro et al., 2004). In intact *Xf*-infected plants, in which the xylem conduits withstand considerable negative pressures, it is likely that an alteration of the pore size like that hypothesized above would lead to an increased probability for air seeding and vessel embolism (Tyree and Zimmermann, 2002; Sperry, 2003), and therefore, to a reduction in the water-conducting capacity of the infected plants. Nevertheless, if more permanent vascular occlusions had not yet developed, air-embolized vessels would refill when infiltrated with water at the relatively high positive pressure used in the K_S tests of excised internodes; e.g. the 103 kPa used in the experiments of Figures 12 and 13. In that situation the hypothesized enzymatic enlargement of the pores may then result in higher water flow rates throughout the stem. This could explain the particularly high K_S values measured in I-N vines (much higher than for healthy control vines; Fig. 13), which were presumably assessed at early stages of infection development when only moderate vessel embolisms were detectable by MRI. In any case, the K_S and MRI data also support the idea that vessel cavitation preceded the development of more permanent vessel occlusions in I-N vines.

There has been disagreement on whether or not the amount of vascular occlusions observed in *Xf*-infected vines is enough to explain the reduction in water-conductive capacity and the other symptoms characteristic of PD (Hopkins, 1989). As in previous studies

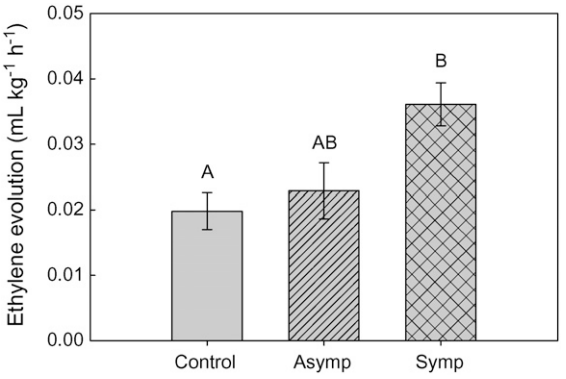

Figure 14. Evolution of ethylene in healthy leaves (Control) from mock-inoculated vines, and in asymptomatic (Asymp) and visually symptomatic (Symp) leaves from *Xf*-inoculated plants. The leaves were enclosed in plastic chambers and ethylene concentration was measured at the end of a 24 h period. The results are expressed as the volume rate of ethylene produced per unit of leaf fresh weight at 25°C. The error lines correspond to ±1 SE, means crowned by different letters are statistically different according to the Tukey-Kramer test ($\alpha = 0.05$). n = 7, 3, and 5 for Control, Asymp, and Symp, respectively.

(Mollenhauer and Hopkins, 1976; Fry and Milholland, 1990), we observed that in infected vines the presence of tyloses and gels is frequent, but that they do not compromise the function of the majority of the vessels. However, our MRI observations of large, dark zones of cavitated vessels in symptomatic stems are coincident with the measured reduction in K_S.

Tyloses, and particularly pectin gels have been observed near or encapsulating bacterial cells in xylem vessels of resistant and tolerant grapevine and muscadine (*Muscadinia rotundifolia*) cultivars (Mollenhauer and Hopkins, 1976; Fry and Milholland, 1990; Krivanek et al., 2005). Thus a divergent role for these vascular occlusions has been suggested. Whereas they can plug vessels and reduce water movement in susceptible cultivars, in resistant genotypes, they can be a defensive mechanism and contribute to the rapid isolation of bacteria, avoiding the systemic spreading of the disease (Mollenhauer and Hopkins, 1976; Hopkins, 1989; Fry and Milholland, 1990). Ethylene production is a common response in many plant-pathogen systems; our results indicate that *Xf*-infected vines also produce more ethylene than healthy vines (Fig. 14). VanderMolen et al. (1983) showed that the exposure of castor bean (*Ricinus communis*) leaf tissue to ethylene can induce pectin gel formation in xylem vessels. Thus, we attempted to learn whether ethylene, in the absence of *Xf*, can cause alterations in stem water transport such as those seen using MRI and K_S analyses of inoculated stems.

In our experiments, grapevines exposed to ethylene demonstrated some of the symptoms observed in PD-infected stems, exhibiting a greater proportion of cavitated vessels and tylose formation, as well as a reduction in the water-conducting capacity. This suggests that, like in other vascular diseases (VanderMolen et al., 1983), ethylene might have a role in the signaling process that leads to the vessel occlusion observed during PD development. However, our test involved treatment of vines with only one, relatively high ethylene concentration. In contrast, our examination of ethylene production by grape leaves, made several weeks after *Xf* inoculation, indicated a much lower level of ethylene production. The more rapid appearance of cavitations following vine ethylene exposure may be explained by this higher exogenous concentration and the fact that exposure was to the entire vine for 48 h. Tests involving treatments of vines with a range of ethylene concentrations/exposure times, and measurements of leaf ethylene production from the time of inoculation are under way.

MATERIALS AND METHODS

Plant Material

The experiments were carried out using grapevines (*Vitis vinifera* cv Chardonnay, clone no. 4), grafted on 110-R rootstocks. The vines were grown in a greenhouse between August, 2003 and June, 2004 in 3.8-L pots. The greenhouse was located at the main campus of the University of California at Davis. No supplementary artificial light was provided, and the average temperature of the room during the period was 21.3°C (minimum 15.2°C and maximum 35.0°C). Plants were supplemented with 100 g of slow-release fertilizer (Osmocote, Scotts-Sierra Horticultural Products) and hand watered as needed, when the surface of the soil had dried out. Most vines had one main shoot with about 15 expanding internodes at the time treatments were initiated.

Inoculation with *Xf*

Seven grapevines were inoculated on September 5, 2003 with *Xf* Temecula strain cultured on PD3 broth and solid medium (Davis et al., 1981). The inoculation was done at the first or second internode from the base of the shoot. Three droplets (20 μL each) of liquid inoculum (10^{-8} colony-forming units mL^{-1}) were placed around the surface of the epidermis with a micropipette and a syringe needle was used to puncture the stem through the center of the droplets until reaching the xylem tissue. The difference in water potential between the xylem and the atmosphere allowed the inoculum to be drawn into the xylem (I vines). The same procedure was used to introduce culture medium (without the bacteria) into the xylem of seven control grapevines (IC vines).

Ethylene Treatment

A custom-built chamber was used to enclose and expose five vines to ethylene (C_2H_4) on September 13, 2003 (E vines). The chamber consisted of a wooden frame (1.2 × 0.6 × 0.6 m) and clear polyethylene walls. A small opening at the top of the chamber provided exchange with the external environment. A mix of ethylene and air (10 μL L^{-1}) was kept flowing into the chamber during 48 h at a rate of 30 L h^{-1}. Small fans were installed at the base of the chamber to ensure adequate gas mixing and circulation throughout the chamber. The room where the chamber was located remained in relative darkness during the treatment (approximately 10 μE m^{-2} s^{-1}). A set of five nontreated (EC) vines, kept in the greenhouse, was used as a control group. Similar treatments were imposed in a previous experiment (January, 2003) on mature Chardonnay vines. Results from this experiment are also presented.

MRI Acquisition

^{1}H-MRI was performed in a 7 Tesla (300 MHz), horizontal wide-bore magnet (180 mm diameter), with a BioSpec spectrometer (Bruker Instruments) located at the Nuclear Magnetic Resonance Facility (University of California at Davis). A microgradient set (60 mm i.d.), capable of approximately 950 mT m^{-1}, was mounted in the magnet bore and a volume coil (35 mm i.d.) was used for both radio frequency (R_F) excitation and reception. The leaves of the vine shoot were held close to the stem and the entire shoot was wrapped with plastic film to allow the introduction of the shoot through the opening of the coil. Then the internode to be imaged was positioned at the center of the volume coil and this assembly placed at the center of the magnet. Ten transverse image slices were simultaneously acquired at the center of the internodes using a gradient-echo pulse sequence, with a tip angle of 30°, a repetition time (T_R) of 500 ms, and an echo time (T_E) of 6.0 ms. Later, only the slice in which the stem was most perpendicularly oriented to the magnetized plane was selected for processing due to its higher image quality. The slices were 1.0 mm thick with a separation of 2.0 mm between them. Adequate signal-to-noise ratio was obtained by averaging four acquisitions per slice. The images were acquired as data arrays of 256 × 256 pixels with a field of view of 12.8 mm (in-plane resolution of 50 μm). Each image required a scanning time of 8 min and 32 s. The gradient-echo method was chosen over spin echo because it provides better contrast due to local field heterogeneity at the boundary of anatomical structures (Blümich, 2000).

The plants were watered and taken to the NMR facility several hours in advance (usually the day before) of being positioned in the magnet. Because of the low evapotranspirational demand of the ambient atmosphere in the facility, this time allowed the water potentials of the plant and the wet soil to equilibrate. Thus any difference observed between the images of treated and control vines (e.g. presence of cavitations) should not be the result of large differences in xylem tensions at the moment of taking the images (Holbrook et al., 2001; Clearwater and Clark, 2003). To produce a series of images depicting the sequential development of air embolisms over several months following inoculation or ethylene exposure, specific internodes were imaged periodically in two treated vines. When clear signs of embolisms were detected in these images (dark zones developed in the xylem), images were

obtained for all the vines and along the entire shoot length. All plants were soon after subjected to destructive K_S measurements. The final acquisition of MRI data started on December 10, 2003 and ended on May 4, 2004 for the inoculation experiment, and for the ethylene experiment it started on January 19, 2004 and finished on June 21, 2004. When the geometry of the stems allowed, images were made at internodes −1, 0, 1, 2, 4, 6, 8, 10, 12, 14, 16, and 18 for the inoculation experiment, considering the inoculation point as internode 0. Internodes 0, 1, 2, 4, 6, 8, 10, 11, 13, 15, 17, 19, and 21 were imaged in the ethylene experiment, where 0 was the most basal internode.

MRI Processing and Image Analysis

MRI raw data sets were zero filled to a matrix of 1,024 × 1,024 pixels and Fourier transformed to produce images with a digital resolution of 12.5 μm, which were converted into TIFF files. These images were further processed and analyzed with the public-domain software package ImageJ version 1.33k (National Institutes of Health, Washington, DC). The background noise was removed from the images using the math tool by subtracting the average background signal intensity +1 SD from the overall signal intensity of the image. Then the tissues to the outside of the vascular cambium, as well as the central pith, were outlined and removed from the images. The area calculator tool was used to quantify the area of the entire xylem disc (A_X).

The images taken along the vines in the inoculation and ethylene experiments were classified in three categories. If the xylem appeared as a disc full of bright vessels, the image was categorized as normal (N). However, if the image was showing one or a few small dark zones indicating that a few vessels were not filled, the image was categorized as having small cavitations (S). If one or more areas of several unfilled vessels were evident, the image was categorized as presenting large cavitations (L).

Tests of MRI Capability to Show Cavitations and Xylem Vessel Content

A series of artificially induced cavitation followed by vessel-refilling experiments was conducted to test whether cavitations could be specifically revealed by our MRI protocol. The stem of a healthy, well-hydrated vine was imaged at a specific, labeled internode. Then the vine shoot was taken out of the magnet to cut and remove a sector accounting for approximately 70% of the stem's cross-sectional area immediately below the imaging site. A second image was then taken at the same position as the first image, where it was anticipated that air would have entered and embolized many vessels. The shoot was again removed from the magnet and the stem segment containing the embolisms and the cut region was excised. This stem segment was refilled with pressurized water introduced through the complete cross section at the base of the segment. An image was made to confirm the refilling of the vessels. Then the stem segment was flushed, in both directions, with pressurized air to completely empty the vessels, and a last image was taken.

We performed an experiment to clarify whether MRI can differentiate between a dilute saline solution (similar to the xylem sap) and pectic materials (components of primary cell walls and plant gels) that can plug water conduits during PD development. Glass tubes containing either a pectin gel, distilled water, or a 10 mM KCl solution were arrayed together in the magnet and imaged using the MRI parameters described previously, except for the field of view that, in this case, was 25.6 mm. The pectin gel was obtained from commercial fruit pectin jelly powder prepared according the instructions of the manufacturer (Sure-Jell, Kraft Foods).

Hydraulic Measurements

Measurements were made within 24 h of finishing the MRI assessments. The shoots were cut at the base and under water to prevent the occurrence of cavitations. While still under water, the cut end was smoothed with a sharp razor blade and fitted tightly to Tygon tubing connected to a plastic reservoir filled with a filtered (0.2 μm) and degassed 10 mM KCl solution. The apical ends of shoots were trimmed back up to internode 17 or 18 from the base, for the ethylene and inoculation experiments, respectively. If the shoots did not have enough internodes they were trimmed up to the last fully expanded internode. The leaf blades were cut and the petioles were sealed using hot plastic glue. Then the reservoir was pressurized at about 103 kPa, forcing the solution into the stem. After waiting 10 to 20 min for a stable flow to be established, the fluid coming out of the apical end was collected in a 10 mL beaker that was weighed after each of three 30 min periods to determine the flow rate (F, kg s^{-1}). F values for whole stems were used to calculate their average specific hydraulic conductivities (K_S, kg m^{-1} s^{-1} MPa^{-1}) according to Equation 1.

$$K_S = \frac{F}{A_S \times \Delta P/\Delta L} \quad (1)$$

ΔP (MPa) represents the pressure differential between the two ends of the stem segment and ΔL (m) is the length of the stem. The term specific refers to the fact that K_S is accounting for differences in the amount of xylem in a given segment by dividing F by the cross-section area of the stem (A_S, m^2; Tyree and Ewers, 1991; Schultz and Matthews, 1993; Tyree and Zimmermann, 2002). Shoot internode segments were excised, discarding about 1 cm of the length containing the nodes. The lengths of the internodes and two orthogonal diameter measurements taken at the center of each segment were recorded. The internodes were connected to the conductivity apparatus and F was determined three times in 30 s intervals. K_S for the individual internodes was also calculated using Equation 1. The stem cross-sectional areas for the internodes were calculated assuming that they were perfect circles, using the average of the internode diameters. An effective whole-stem cross-sectional area was calculated as the length-weighted average for all the internodes in the shoot. A dilute salt solution rather than pure water was used in the measurements to prevent sharp drops in F (van Ieperen et al., 2000; Zwieniecki et al., 2001; Tyree and Zimmermann, 2002).

The reciprocal of K_S ($1/K_S$) is defined as the specific hydraulic resistivity (ρ_S), which is an indication of how difficult it is for the KCl solution to move through the stem. The electric circuit analogy for water flow indicates that the summation of the individual resistors in a circuit in series is equal to the total resistance of the circuit. Mathematical manipulations of this property allowed us to partition the total resistivity in a stem (ρ_{STEM}) between the internode (ρ_{INT}) and node (ρ_{NODE}) components; this also was applied to estimate ρ_{NODE} values, which were not measured. The hydraulic resistance through a path is defined as the pressure differential (ΔP) divided by F. The relationship between the hydraulic resistance of the whole stem (R_{STEM}), the internode resistance (R_{INT}), and the node resistance (R_{NODE}) is represented in Equation 2.

$$R_{STEM} = R_{INT} + R_{NODE} \quad (2)$$

Normalizing R_{STEM} by the effective cross-section area (A_{STEM}), calculated as the length-weighted average of the cross sections for all the internodes in the stem, and the length of the stem (L_{STEM}) results in ρ_{STEM}. Equation 3 is the result of multiplying both sides of Equation 2 by A_{STEM}/L_{STEM}, the term on the left side represents ρ_{STEM}.

$$\frac{A_{STEM}}{L_{STEM}} \times R_{STEM} = \frac{A_{STEM}}{L_{STEM}}(R_{INT} + R_{NODE}) \quad (3)$$

R_{INT} is compounded from the resistances in series for each internode in the stem. Changing R_{STEM} by using the definition of hydraulic resistance and expressing R_{INT} as the summation of the resistances of all the individual internodes allowed us to obtain Equation 4, where ΔP_i is the pressure differential across the internode segments (103 kPa for all) and F_i represents the water flow rate of each internode.

$$\frac{A_{STEM}}{L_{STEM}} \times \frac{\Delta P_{STEM}}{F_{STEM}} = \frac{A_{STEM}}{L_{STEM}}\left(\sum \frac{\Delta P_i}{F_i} + R_{NODE}\right) \quad (4)$$

Equation 5 was obtained by rearranging terms in Equation 4 and expressing some of them as resistivities. Equation 5 shows the calculation procedure used to estimate ρ_{NODE} from the data collected in our measurements.

$$\rho_{NODE} = \rho_{STEM} - \frac{A_{STEM}}{L_{STEM}} \times \sum \frac{\Delta P_i}{F_i} \quad (5)$$

Hydraulic resistance values for all internodes are required to compute ρ_{INT} for a particular stem. Missing resistances for distal internodes (Fig. 13) were estimated by averaging the inverse of the K_S values for the internodes located above and below the internodes for which resistance measurements were missing. That number was then corrected by the internode cross-section area and length, which were measured for all the internodes, to obtain a resistance. Also ρ_{INT} can be more formally calculated using the definition for resistivity as $\frac{A_{INT}}{\sum L_i} \sum \frac{\Delta P_i}{F_i}$ where A_{INT} is the average cross section of all the internodes and L_i is the length of the individual internodes. This method yielded values very

similar to those obtained using the far-right side of Equation 5. This indicates that Equations 3 to 5 are adequate for estimating ρ_{NODE} and partitioning ρ_{STEM} between ρ_{INT} and ρ_{NODE}.

Light Microscopy

Excised internodes from treated and control plants were fixed in formalin, acetic acid, and alcohol (Johansen, 1940). The samples were subjected to an alcohol dehydration series using a mild vacuum to remove the air at each step (Brooks et al., 1950) and then infiltrated and embedded in Paraplast Extra paraffin (Fisher HealthCare). The blocks of embedded tissue were sectioned at 10 μm with a Leica 2155 rotary microtome (Leica). Two slides of sectioned material were made of each sample. The sections on one slide were stained using toluidine blue-O, a stain for general anatomical study, whereas the sections on the second slide were stained with coriphosphine-O, a fluorescent stain for pectins (Weis et al., 1988). Finished slides were observed under the compound microscope and digital images were acquired.

Ethylene Measurements

Healthy leaves from mock-inoculated plants (control), nonsymptomatic (asymp), and visually symptomatic (symp) leaves from infected plants, were detached and immediately incubated in custom-built, flat, Plexiglas chambers ($200 \times 205 \times 20$ mm, 450 mL internal volume). The leaves weighed about 4 g each. In visually symptomatic leaves approximately 30% of the lamina presented chlorosis, some leaves also presented small necrotic spots. One milliliter gas samples from the chamber's headspace were taken through a septum fitted in the wall of the chambers and injected into a gas chromatograph Carl 211 (Chandler Engineering) equipped with an F-1 alumina column and a flame ionization detector. Nitrogen gas at 30 mL min^{-1}, 80°C was used as carrier.

Statistical Analysis

The data were analyzed using the statistical package JMP, version 5.1 (SAS Institute). A one-way ANOVA test was used to analyze the differences between the means of inoculation and ethylene treatments, and the controls. The one-sided version of the test was used in Figures 12 and 13 to determine if the treatments had higher ρ_S or lower K_S means than the controls. When necessary, an inverse transformation was performed on the K_S data to meet the assumption of homoscedasticity of variances among treatments. However, the untransformed data were presented in the figures and in the "Results" section (Sokal and Rohlf, 1995). The means for ethylene production in the different leaf groups were analyzed using ANOVA and further separated by the Tukey-Kramer multiple comparison test. For the continuous variables A_S and A_X, linear regression analysis was used. The images (MRI) obtained along the stems of the different treatments were categorized (N, S, and L). Contingency and correspondence analyses and the likelihood-ratio χ^2 test were used to analyze the distribution of the proportions of each category across the treatments.

ACKNOWLEDGMENTS

We thank Duarte Nurseries for their generosity in providing the grapevines used in this research, Dr. Caroline Roper for assistance in preparing the *Xf* cultures used for inoculation of grapevines, Dr. Katie Pinney for invaluable guidance in performing the histochemical analysis of stem tissues, Mr. Joshua Lenhof for assistance with sample handling and histochemical analysis, and Professor Wendy Silk for her careful reading of the manuscript and useful suggestions.

Received July 21, 2006; accepted December 1, 2006; published December 22, 2006.

LITERATURE CITED

Agüero CB, Uratsu SL, Greve C, Powell ALT, Labavitch JM, Meredith CP, Dandekar AM (2005) Evaluation of tolerance to Pierce's disease and *Botrytis* in transgenic plants of *Vitis vinifera* L. expressing the pear PGIP gene. Mol Plant Pathol **6:** 43–51

Blümich B (2000) NMR Imaging of Materials. Oxford Science Publications, New York

Brooks RM, Bradley MV, Anderson TI (1950) Plant Microtechnique Manual. University of California, Davis, CA

Clearwater MJ, Clark CJ (2003) *In vivo* magnetic resonance imaging of xylem vessel contents in woody lianas. Plant Cell Environ **26:** 1205–1214

da Silva FR, Vettore AL, Kemper EL, Leite A, Arruda P (2001) Fastidian gum: the *Xylella fastidiosa* exopolysaccharide possibly involved in bacterial pathogenicity. FEMS Microbiol Lett **203:** 165–171

Davis MJ, French WJ, Schaad NW (1981) Axenic culture of the bacteria associated with phony disease of peach and plum leaf scald. Curr Microbiol **6:** 309–314

Fry SM, Milholland RD (1990) Response of resistant, tolerant and susceptible grapevine tissues to invasion by the Pierce's bacterium, *Xylella fastidiosa.* Phytopathology **80:** 66–69

Hacke UG, Sperry JS, Pittermann J (2000) Drought experience and cavitation resistance in six shrubs from the Great Basin, Utah. Basic Appl Ecol **1:** 31–41

Holbrook NM, Ahrens ET, Burns MJ, Zwieniecki MA (2001) In vivo observation of cavitation and embolism repair using magnetic resonance imaging. Plant Physiol **126:** 27–31

Hopkins DL (1989) *Xylella fastidiosa*: xylem-limited bacterial pathogen of plants. Annu Rev Phytopathol **27:** 271–290

Johansen DA (1940) Plant Microtechnique. McGraw-Hill, New York

Krivanek AF, Stevenson JF, Walker MA (2005) Development and comparison of symptom indices for quantifying grapevine resistance to Pierce's disease. Phytopathology **95:** 36–43

Lo Gullo MA, Trifilo P, Raimondo F (2000) Hydraulic architecture and water relations of Spartium junceum branches affected by a mycoplasm disease. Plant Cell Environ **23:** 1079–1088

McElrone AJ, Sherald JL, Forseth IN (2003) Interactive effects of water stress and xylem-limited bacterial infection on the water relations of a host vine. J Exp Bot **54:** 419–430

Mollenhauer HA, Hopkins DL (1976) Xylem morphology of Pierce's disease-infected grapevines with different levels of tolerance. Physiol Plant Pathol **9:** 95–100

Mollenhauer HH, Hopkins DL (1974) Ultraestructural study of Pierce's disease bacterium in grape xylem tissue. J Bacteriol **119:** 612–618

Newbanks D, Bosch A, Zimmermann MH (1983) Evidence of xylem dysfunction by embolization in Dutch elm disease. Phytopathology **73:** 1060–1063

Newman KL, Almeida RPP, Purcell AH, Lindow SE (2003) Use of a green fluorescent strain for analysis of *Xylella fastidiosa* colonization of *Vitis vinifera.* Appl Environ Microbiol **69:** 7319–7327

Newman KL, Almeida RPP, Purcell AH, Lindow SE (2004) Cell-to-cell signaling controls *Xylella fastidiosa* interactions with both insects and plants. Proc Natl Acad Sci USA **101:** 1737–1742

Osiro D, Colnago LA, Otoboni AMMB, Lemos EGM, de Souza AA, Filho HDC, Machado MA (2004) A kinetic model for *Xylella fastidiosa* adhesion, biofilm formation, and virulence. FEMS Microbiol Lett **236:** 313–318

Scarpari LM, Lambais MR, Silva DS, Carraro DM, Carrer H (2003) Expression of putative pathogenicity-related genes in Xylella fastidiosa grown at low and high cell density conditions in vitro. FEMS Microbiol Lett **222:** 83–92

Schultz HR, Matthews MA (1993) Xylem development and hydraulic conductance in sun and shade shoots of grapevine (*Vitis vinifera* L.): evidence that low light uncouples water transport capacity from leaf area. Planta **190:** 393–406

Simpson AJG, Reinach FC, Arruda P, Abreu FA, Acencio M, Alvarenga R, Alves LMC, Araya JE, Baia GS, Baptista CS, et al (2000) The genome sequence of the plant pathogen *Xylella fastidiosa.* Nature **406:** 151–157

Sokal RR, Rohlf FJ (1995) Biometry. The Principles and Practice of Statistics in Biological Research, Ed 3. Freeman, New York

Sperry JS (2003) Evolution of water transport and xylem structure. Int J Plant Sci **164:** S115–S127

Stevenson JF, Matthews MA, Greve LC, Labavitch JM, Rost TL (2004) Grapevine susceptibility to Pierce's disease II: progression of anatomical symptoms. Am J Enol Vitic **55:** 238–245

Tyree MT, Ewers FW (1991) Tansley review no. 34: the hydraulic architecture of trees and other woody plants. New Phytol **119:** 345–360

Tyree MT, Zimmermann MH (2002) Xylem Structure and the Ascent of Sap, Ed 2. Springer, Berlin

van Ieperen W, van Meeteren U, van Gelder H (2000) Fluid ionic composition influences hydraulic conductance of xylem conduits. J Exp Bot **51:** 769–776

VanderMolen GE, Labavitch JM, Strand LL, DeVay JE (1983) Pathogen-induced vascular gels: ethylene as a host intermediate. Physiol Plant **59:** 573–580

Varela LG, Smith RJ, Phillips PA (2001) Pierce's Disease. Publication 21600. University of California, Division of Agricultural and Natural Resources, Oakland, CA

Weis KG, Polito VS, Labavitch JM (1988) Microfluorometry of pectic materials in the dehiscence zone of almond (Prunus dulcis [Mill.] DA Webb) fruits. J Histochem Cytochem **36:** 1037–1041

Wulff NA, Carrer H, Pascholati SF (2003) Cloning and expression of cellulase XF-818 of *Xylella fastidiosa* in *Escherichia coli*. Scientia Agricola **60:** 715–721

Zwieniecki MA, Melcher PJ, Holbrook NM (2001) Hydrogel control of xylem hydraulic resistance in plants. Science **291:** 1059–1062